crystals

MDPI

Article

Room-Temperature Synthesis of Tubular Hexagonal Boron Nitride under Pressure

Junkai Li *, Donghan Jia, Guoliang Niu, Peiyang Mu and Huiyang Gou

Center for High Pressure Science and Technology Advanced Research, Beijing 100193, China; donghan.jia@hpstar.ac.cn (D.J.); guoliang.niu@hpstar.ac.cn (G.N.); peiyang.mu@hpstar.ac.cn (P.M.); huiyang.gou@hpstar.ac.cn (H.G.)

* Correspondence: junkai.li@hpstar.ac.cn

Abstract: Hexagonal boron nitride (h-BN) exhibits interesting optical and mechanical properties, including chemical and thermal stability. Extensive techniques have been applied for the realization of h-BN at high temperatures. Here, we propose a room-temperature preparation of h-BN at high pressure through the compression of ammonium azide and boron powder. The structure and morphology of the obtained h-BN are found to possess tubular-like features, and the selected-area electron diffraction and electron energy-loss spectroscopy support the formation of h-BN. Remarkably, h-BN grows gradually from the surface of boron particles to form a core–shell structure. This tubular morphology of h-BN with a size of 70 nanometers in length and 27 nanometers in width differs from the conventional lamellar h-BN generated with temperature assistance. Our results demonstrate a method for the room-temperature synthesis of tubular h-BN, which shows great promise for the preparation of other nitrides at high pressure and room temperature.

Keywords: high-pressure synthesis; chemical reaction; hexagonal boron nitride

Citation: Li, J.; Jia, D.; Niu, G.; Mu, P.; Gou, H. Room-Temperature Synthesis of Tubular Hexagonal Boron Nitride under Pressure. *Crystals* **2023**, *13*, 1201. https://doi.org/10.3390/cryst13081201

Academic Editors: Simone Anzellini, Daniel Errandonea, Anna Herlihy and Robin Turnbull

Received: 8 July 2023
Revised: 25 July 2023
Accepted: 31 July 2023
Published: 2 August 2023

1. Introduction

Hexagonal boron nitride (h-BN) exhibits a wide optical band gap, high thermal conductivity, and chemical stability, making it an extremely promising material for the development of advanced electrical and optical devices [1–6]. In industry, h-BN is commonly obtained from boric acid and ammonia, and high-temperature pyrolysis (sometimes over 1000 °C) and purification are needed to obtain high-quality h-BN [7–9]. The chemical vapor deposition (CVD) method is another common approach for synthesizing h-BN, typically requiring a suitable substrate for the growth of well-formed h-BN with a reaction temperature typically above 800 °C [10–14]. In general, these methods have been used for producing polycrystalline h-BN, but the preparation of high-purity and large-size single-crystal h-BN remains a challenge. Single-crystal h-BN can be synthesized at a pressure of 3 GPa and a temperature of over 1900 K by using highly active alkali metal salts as precursors. Single crystals of hexagonal boron nitride can reach up to 2 cm in size using high-pressure and high-temperature (HPHT) techniques [15,16]. Over the decades, scientists have strived to develop new methods for synthesizing h-BN. One approach involves preparing boron nitride through a molten salt, which utilizes $NaBF_4$ and $NaNH_2$ in a lithium bromide melt [17]. Moreover, scientists have devised a benzene-thermal technique for cultivating h-BN, in which the lowest temperature is only 350 °C [18].

However, up to now, no methods have been reported for the realization of h-BN at room temperature. Additionally, h-BN is inherently inert, and its oxidation resistance temperature can exceed 900 °C [19]. In thermochemical reactions, temperature serves as the driving force for the reaction, and the increase in temperature intensifies the thermal motion of the reacting molecules, leading to more reactant molecules being activated and subsequently reacting to produce new molecules [20]. Besides the temperature, pressure can reduce the distances between reactant molecules, modify their electronic orbitals, and

increase the reactivity of compounds, thus enhancing the driving force of the reaction. Unusual phenomena can be revealed when substances are subjected to high pressure; for instance, metallic sodium becomes transparent under extreme conditions [21]. Pressure can also be used as a driving force to induce polymerization, such as in the formation of nanowires from benzene and pyridine. Under high pressure, molecules such as benzene and pyridine are squeezed together. Upon reaching a critical distance, hydrogen atoms are forced out of the molecule, and the unsaturated carbon bonds form, resulting in the development of an ordered crystalline structure. It is hypothesized that other hydrogen-containing compounds may also have critical points under extreme pressure, where hydrogen may be expelled and new chemical bonds formed [22–24].

Here, we propose a room-temperature synthesis of h-BN using ammonium azide and boron nanopowder as reactants, with pressure as the only driving force of the chemical reaction. In the experiments, the nitrogen source was the ammonium azide (NH_4N_3), which is highly reactive and decomposable during the experiments. Nanoboron powder with a large specific surface area provides the numerous reaction sites, ensuring a rapid and complete reaction. The obtained products exhibit a unique core–shell structure with nanoboron particles as the central "core" and h-BN as the "shells", with a tubular morphology. The tubular h-BN is approximately 70 nanometers in length and 27 nanometers in width, and it is stacked with approximately 20–30 layers of monolayer boron nitride. This tubular h-BN is distinctive from the lamellar structure produced by traditional auxiliary heating methods. Furthermore, EELS mapping and elemental quantitative analysis indicate that the tubular morphology region has equal proportions of nitrogen and boron atoms. Additionally, its EELS spectrum exhibits characteristic π* and σ* peaks of both boron and nitrogen, which confirm the formation of sp^2 valence bonds between them. The position of the absorption peaks of the obtained sample are consistent with that of commercial h-BN, strongly validating the successful synthesis of h-BN at room temperature and high pressure. The room-temperature synthesis of h-BN proposed here may broaden the synthetic methods of boron nitride and also provides insights for the realization of other nitrides.

2. Materials and Methods

The starting nanoboron powder with a purity of 99.9% was purchased from Aladdin Reagent Co., Ltd., Shanghai, China, and ammonium azide was produced by the reaction of sodium azide or magnesium azide with ammonium chloride. To analyze the precursor and samples, X-ray diffraction (XRD) was performed using a powder X-ray diffractometer (D8 Discover, Bruker) with CuKα radiation. The goniometer was calibrated using high-purity silicon with a lattice parameter of 5.4311 Å. Nanoboron powder was found to be consistent with β-boron (space group: R-3m, Figure S1, see in Supplementary Materials), and the nanoboron powder displayed excellent crystallinity and was free of impurities. With regard to the ammonium azide, its diffraction peaks match with Pmna symmetry (Figure S2), indicating high crystallinity.

High-pressure experiments were conducted using a diamond anvil cell (DAC) and a Kawai-type multianvil press at the Center for High Pressure Science and Technology Advanced Research. A DAC with a culet size of 300 μm was used for Raman measurements at room temperature. The mixture of nanoboron powder and ammonium azide was loaded into a hole of the Re gasket (150 μm hole diameter). The pressure was calibrated using the ruby fluorescence method. Raman spectra were recorded in a backscattering geometry using a Spectrometer (LabRam HR Evolution Horiba, Paris, France) with a laser of 532 nm wavelengths (the focus spot size was about 5 μm, the laser power was 0.182 mW, and the acquisition time was 60 s).

The synthesis was performed in a Kawai-type multianvil press with a 7/3 assembly (shown in Figure 1a). The press was slowly ramped up at a hydraulic pressure of 1 bar/min, held for two hours after reaching the target pressure, and then decompressed at a rate of 2 bar/min. As shown in Figure 1b,c, nanoboron powder reacts with ammonium azide to synthesize h-BN under pressure. The pressure setting was estimated based on the P-T

calibration curves, which were calibrated by the phase transition of ZnS (15.6 GPa), ZnTe (18.8 GPa), and GaP (22.5 GPa) at room temperature. Furthermore, the Al_2O_3 content in bridgmanite (quenched sample from 2000 K at high pressure) was measured to calibrate the pressure of more than 27 GPa [25–28]. Temperature was measured simultaneously using a D-type thermocouple (W3%Re–W25%Re) while heating at high pressure. A homogeneous mixture of ammonium azide and nanoboron powder was quickly loaded into a Pt capsule (1.6 mm in diameter, 1.8 mm in height). The initial mixture was compacted and then tightly sealed to prevent decomposition of the ammonium azide.

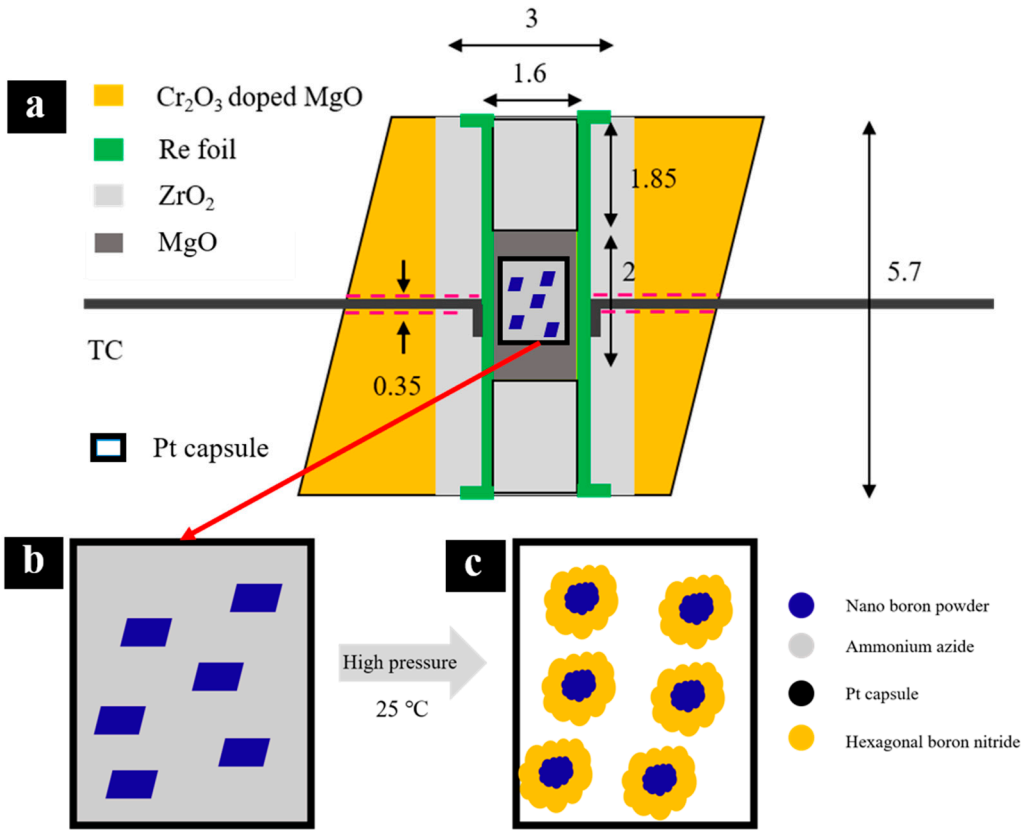

Figure 1. Schematic diagram of (**a**) high-pressure assembly in the multianvil press; (**b**) starting material; and (**c**) recovered products in the Pt capsule.

Morphological characterization was performed using a scanning electron microscope (FESEM, JSM-7900F, JEOL Co., Ltd., Tokyo, Japan) with a working distance of 10 mm and an acceleration voltage of 15 kV. The samples were placed on an SEM holder. To minimize the charge accumulation on the surface of the sample, a Pt coating was applied before imaging, due to the weak conductivity of boron nitride. The powder samples were dispersed in ethanol and subjected to ultrasonic treatment to obtain a uniform suspension, which was then dropped onto the copper grid. The morphology and structure of the samples were characterized by high-resolution transmission electron microscopy (HR-TEM) and selected-area electron diffraction (SAED) using a TEM (JEM-F200, JEOL Co., Ltd., Tokyo, Japan) with an accelerating voltage of 200 kV. Electron energy-loss spectrum (EELS) measurements were performed in a condenser spherical aberration-corrected TEM (JEM-ARM300F, JEOL Co., Ltd., Tokyo, Japan), with an accelerating voltage of 300 kV.

3. Results and Discussion

3.1. In Situ High-Pressure Raman Spectroscopy

The reaction was performed using ammonium azide and nanoboron powder with a proportion of boron and nitrogen of 1:4 (molar ratio). The mixture was placed in a DAC sample chamber and subjected to in situ Raman spectroscopy under pressure to

monitor the potential changes. As shown in Figure 2, initially, the Raman vibrational peak around 1350 cm^{-1} of N_3^- in ammonium azide overlaps with the vibrational peak of diamond anvils. As the pressure increases, the N_3^- peak gradually separates from the diamond peak and shifts to a higher frequency [29]. As the pressure increases to 17.5 GPa, a new peak appears around 1370 cm^{-1}, which may be related to a boron–nitrogen sp^2 bonding vibration peak [30–33]. In contrast, no peak splitting or new peaks were observed in ammonium azide up to a pressure of 85.3 GPa [34]. The peak of N_3^- continues to shift to a higher frequency and decreases in intensity, consistent with the literature [34,35]. Simultaneously, the Raman vibrational peak shifts to a higher frequency with increasing pressure. At 36.5 GPa, the peak shifts by 40 cm^{-1}, to around 1409 cm^{-1}.

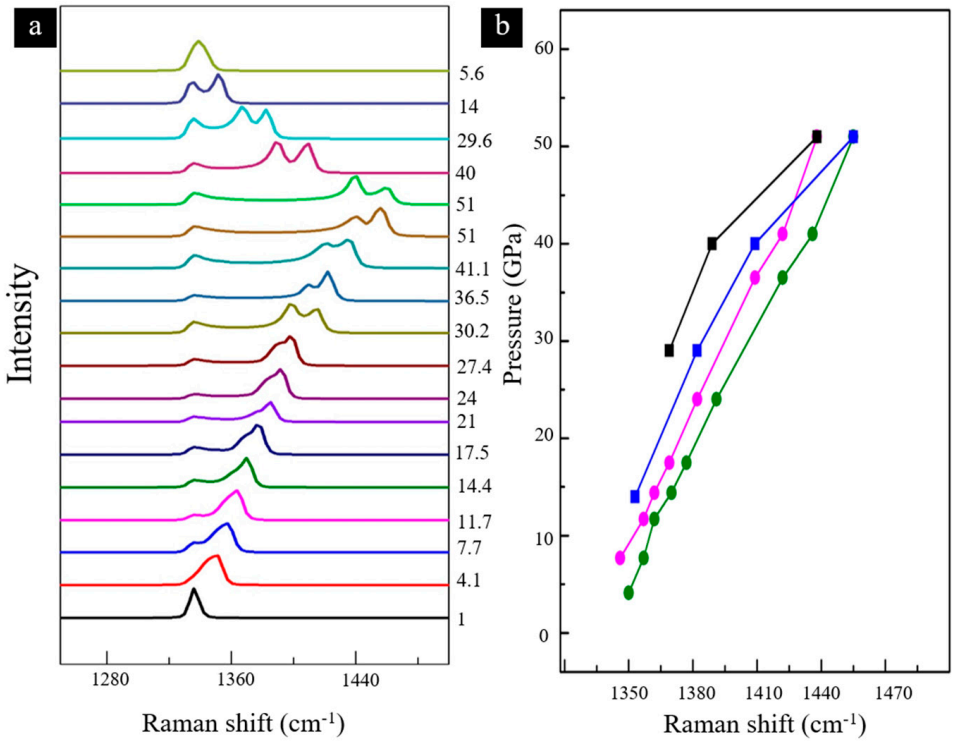

Figure 2. (**a**) In situ Raman vibrational peak as a function of pressure of the mixture of ammonium azide and nanoboron powder at room temperature; (**b**) variation in Raman peaks of boron-nitrogen sp^2 bond (pink and black lines) and N_3^- with pressure (green and blue lines).

Upon decompression, as presented in Figure 2a, the vibrational peaks in the Raman spectrum undergo a red shift. When the pressure drops to 14 GPa, the Raman vibration of the nitrogen–boron bond disappears, which indicates a reversible reaction between ammonium azide and nanoboron powder. This phenomenon may be similar to the stripping process of valence bonds of single-crystal graphite under pressure [22,36]. Figure 2b shows the changes in Raman shifts of the nitrogen-boron sp^2 bond (red and black polylines) and N_3^- (green and blue polylines) during the compression and decompression process. The Raman shift shows nonlinear changes, indicating that ammonium azide may react with boron to form new products.

3.2. Morphology and Structural Characterizations

To fully understand the room-temperature synthesis of h-BN, we conducted the experiments using a multianvil press with a relatively large sample size. We compressed a mixture of ammonium azide and nanoboron powder to 28 GPa, which was maintained for two hours before being recovered to ambient conditions. Figure S3 shows the optical photographs of the obtained samples. The products obtained at 28 GPa and room temperature show a brownish-yellow color, while the nano boron powder exhibits a grayish-black color,

which supports a possible chemical reaction under pressure. As a contrast, the commercial boron nitride (Figure S3d) exhibits a typical white color. X-ray diffraction (XRD) pattern analysis was performed on the samples obtained from 28 GPa and room temperature. As illustrated in Figure S4, the black lines correspond to β-boron (PDF#80-0323), and the red lines correspond to h-BN (PDF#73-2095). By comparing the XRD patterns of the recovered samples and β-boron, the recovered sample is found to exhibit a diffraction peak with significant broadening at approximately 26°, as indicated by the dashed box area in Figure S4. This broadened peak can be attributed to the (002) diffraction peak of h-BN, which is likely due to the low content of the sample and its poor crystallinity [37,38].

Before the synthesis, the precursor of nanoboron powder shows a lamellar morphology with a smooth surface (Figure 3a), and the particle size is approximately 100–500 nm. After compression, the sample presents two typical morphologies according to SEM images. As shown in Figure 3a–c, the stacking of lamellae and a tubular morphology are presented in the recovered products. Energy-dispersive X-ray spectroscopy (EDS) was performed on two regions, and the results are shown in Figure 3d. The size of the lamellae is approximately a few hundred nanometers. The EDS observation shows that the B:N atomic ratio in this region is 84.4%:15.6%. The red dashed box shows fine tubular shapes, with burr monomer sizes of approximately 100 nm. The EDS tests revealed an atomic ratio of 76.7%:23.3% for B and N in this area.

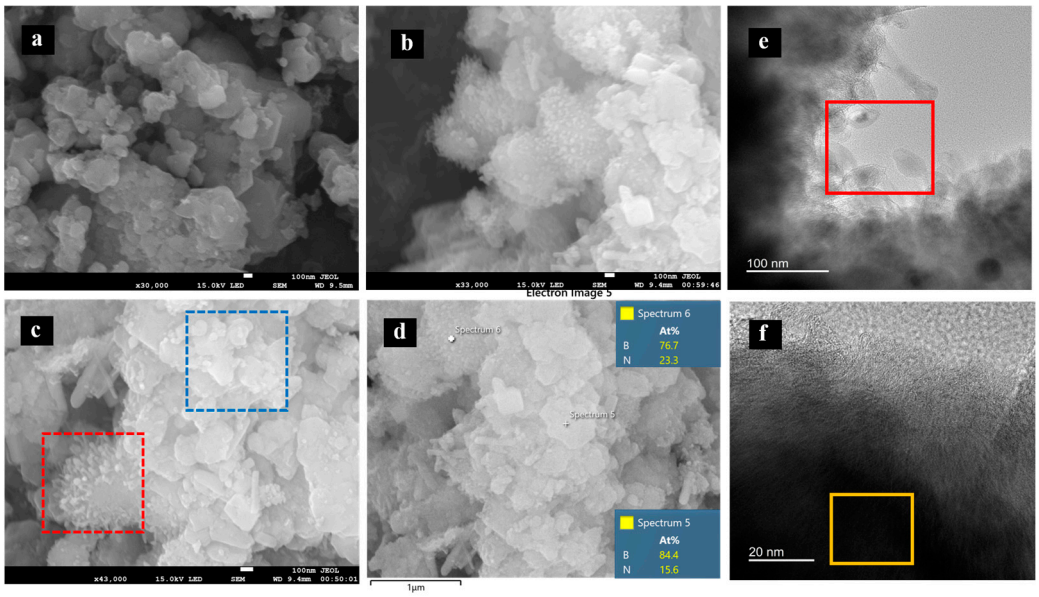

Figure 3. (**a**) SEM images of nanoboron powder; (**b**) SEM images at different magnifications of obtained sample synthesized under 28 GPa at room temperature; (**c**) different morphologies of tubular area (red box) and layered areas (blue box); (**d**) ratio of nitrogen and boron content at different areas; (**e**,**f**) morphology and element content of tubular morphology area (red box) and lamellar morphology area (yellow box).

The nitrogen content in the region with tubular morphology was significantly higher than that of the region with the lamellar morphology. These results show that there are no distinct regions within the acquired samples that contain solely boron. This phenomenon suggests that the nanoboron particles have been completely integrated with ammonium azide. Furthermore, the proportion of boron and nitrogen elements varies across different morphological regions, indicating that the sample is still a mixture. Transmission electron microscope (TEM) observations show that the tubular morphology region features vesicle and tubular morphologies (Figure 3e). The size of these structures falls within the range of 50–100 nm, which is in agreement with the SEM results. The atomic ratio of boron to nitrogen from TEM-EDS was found to be 47%:53% (Table 1). Therefore, it can be determined that the material with the tubular morphology is a highly pure form of h-BN [39]. Unlike

ammonia-borane, the combined precursor of ammonium azide and boron powder does not have any boron–nitrogen bonding; the generation of h-BN signifies that pressure is the only factor driving B–N bond formation. The layered morphology of the yellow box region in Figure 3f shows that the boron to nitrogen ratio in this area is 90%:10% (Table 1), indicating that most of the flaky material is the unreacted nanoboron powder. The statistics of the relevant TEM-EDS data are presented in Table S1.

Table 1. Atomic percentage of boron and nitrogen content in different regions in Figure 3e,f.

Element	Atomic Ratio (Red Area)	Atomic Ratio (Yellow Area)
B	46.9 ± 0.8%	90.4 ± 0.7%
N	53.1 ± 0.8%	9.6 ± 0.7%
Total	100%	100%

For a better understanding of the composition and morphology of the obtained sample, an individual particle was chosen for observation under TEM (Figure 4a). A statistical analysis on the size of the synthesized sample was performed and the results show that the average size of the obtained particles is around 0.23 um; the SEM image and statistical chart are shown in Figure S6. Figure 4a depicts several particles that appear to be stacked together, with an estimated size of approximately 500 nanometers for these boron particles, and they are enveloped by the tubular morphology of h-BN on its surface. The particles feature a core–shell structure with h-BN forming a shell wrapped around the surface of the boron particle. The tubular morphology of h-BN is densely packed and adhered around the boron particles, and it has a length of approximately 70 nm and a width of about 27 nm. The diameter and length statistics of the size of boron nitride were calculated and are shown in Figures 4a and S5. The average diameter of the tubular boron nitride synthesized at room temperature is about 26.8 nm, and the average length is about 70.8 nanometers. In addition, the boron particle area was tested, and the lattice distance of boron was measured to be 0.44 nm, consistent with the (202) basal plane of β-boron (Figure 4c). In Figure 4c, we can see significant differences in the structure of different regions. The morphology and structure of the synthesized sample could be divided into three typical regions: the highly crystalline β-boron region, the amorphous intermediate region, and the h-BN region with tubular morphology. Under high pressure, ammonium azide gradually infiltrates boron nanoparticles, destroying the lattices and reacting with the boron to generate h-BN. The crystalline boron serves both as a skeleton and a reactant, and, based on its unique morphology, the growth process may be similar to the initial process of boron nitride nanotubes in traditional methods. [40–42].

To further understand the structure of the h-BN with a tubular morphology, selected-area electron diffraction was conducted (as shown in Figure 5a). The weak diffraction ring suggests the broadening of diffraction peaks, indicating the poor crystallinity of the generated h-BN. The corresponding lattice spacing is obtained by measuring the distances from the diffraction ring to the center of the transmission spot. In Figure 5a, the marks indicate that the lattice distances of the two brightest diffraction rings of about 0.336 nm and 0.21 nm correspond to the (002) and (110) crystal planes of h-BN. Zooming in on the vesicle structures, the layered-like structure can be easily observed in Figure 5b. The vesicle structures consist of approximately 20–25 mono-layers of (002) of h-BN, indicating that boron reacts with ammonium azide under high pressure and gradually assembles to produce h-BN with a multilayer tubular morphology. Some areas show a relatively messy form, which is a chaotic stacking of layered materials (Figure 5c). The lattice distance of the material is approximately 0.336 nm, which corresponds to the (002) crystal plane of h-BN (as depicted in Figure 5d).

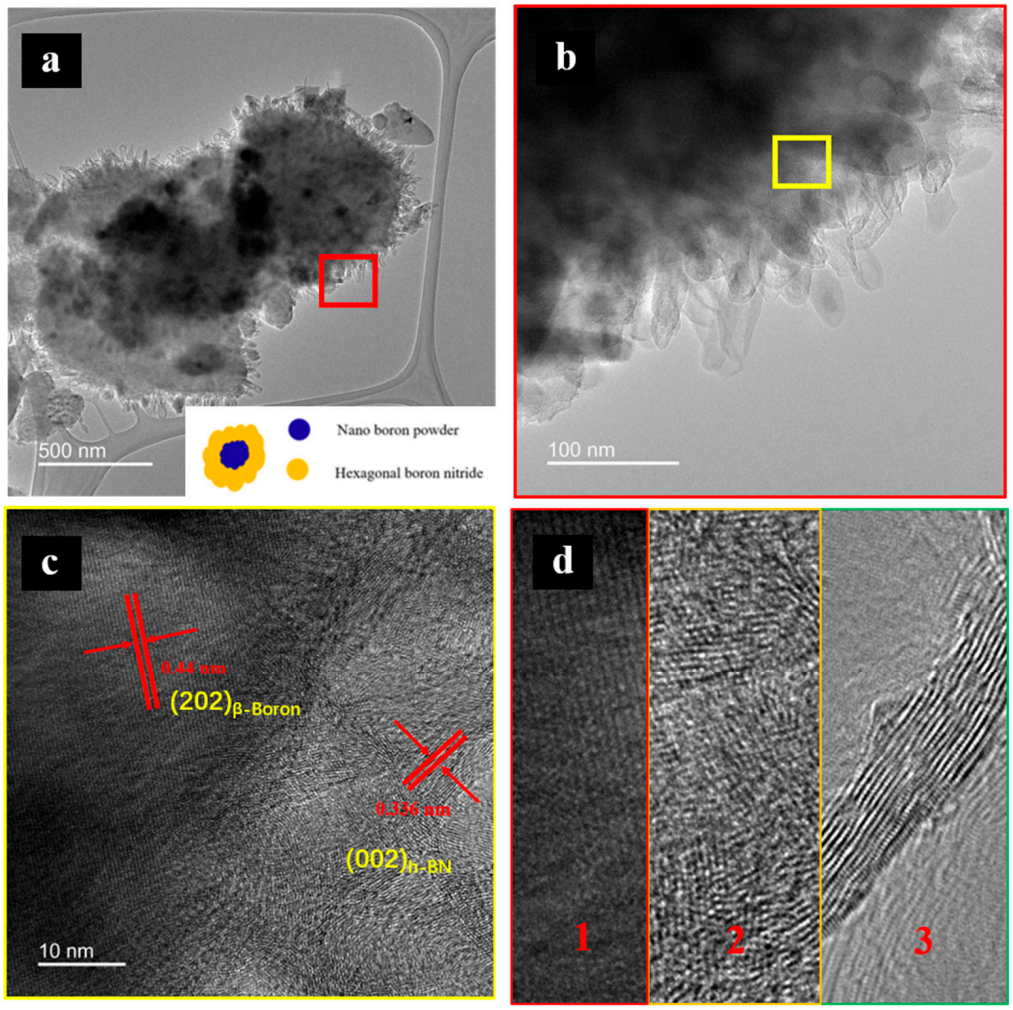

Figure 4. (**a**) TEM image of obtained sample; (**b**) TEM image of tubular morphology; (**c**) TEM image of two-phase boundary of boron and boron nitride; (**d**) TEM image of burr-shaped h-BN (Zone 1: crystal boron; Zone 2: amorphous complex; Zone 3: layered boron nitride).

Electron energy-loss spectroscopy (EELS) mapping was conducted on the synthesized samples in order to obtain the contents of nitrogen and boron elements. The tubular shape depicted in Figure 6b exhibits a distinct uniformity in the distribution of boron and nitrogen elements. Additionally, from the perspective of color contrast, there appears to be no discernible segregation of either boron or nitrogen within the structure. Quantitative analysis was carried out in three different structural regions. A total of five points were taken from the end of the tube to the boron "core" of the sample particle (Figure 6c,d). The nitrogen-to-boron element ratio in the tubular morphology area was about 1:1, revealing almost constant ratios in different regions with h-BN of a tubular morphology (Figure 6d). Interestingly, the junction between the tubular and crystal boron particle regions has a substantially lower content of nitrogen, indicating that this region is a mixture of hexagonal boron nitride and boron. Combined with the results in Figures 4c and 6b, our results provide compelling evidence that ammonium azide undergoes a gradual reaction with crystalline boron, ultimately resulting in the formation of tubular boron nitride. The boron "core" region contained about 14% nitrogen, which may belong to the amorphous intermediate region as shown in Figure 4d. EELS analysis was carried out on commercial h-BN to enable a better comparison with the obtained sample. Figure S8 depicts that the atomic proportions of nitrogen and boron are obtained by integrating the red region. Our results reveal that the atomic ratios of nitrogen and boron are consistent with the particles of commercial h-BN (Figure S8). In general, h-BN can be synthesized using various methods,

including traditional high-temperature pyrolysis, chemical vapor deposition, and solvothermal methods [43]. The traditional high-temperature pyrolysis method is commonly used in industrial synthesis and typically results in irregular lamellar morphology. Chemical vapor deposition and solvothermal methods can produce more regular morphologies, with triangular or hexagonal shapes and homogeneous lamellar sizes. While the chemical vapor deposition method can produce high-quality hexagonal boron nitride nanotubes with good crystallinity, it typically requires a high reaction temperature and the use of catalysts such as magnesium borate [44]. However, the room temperature and high-pressure synthesis produces a special tubular morphology that is distinct from traditional methods.

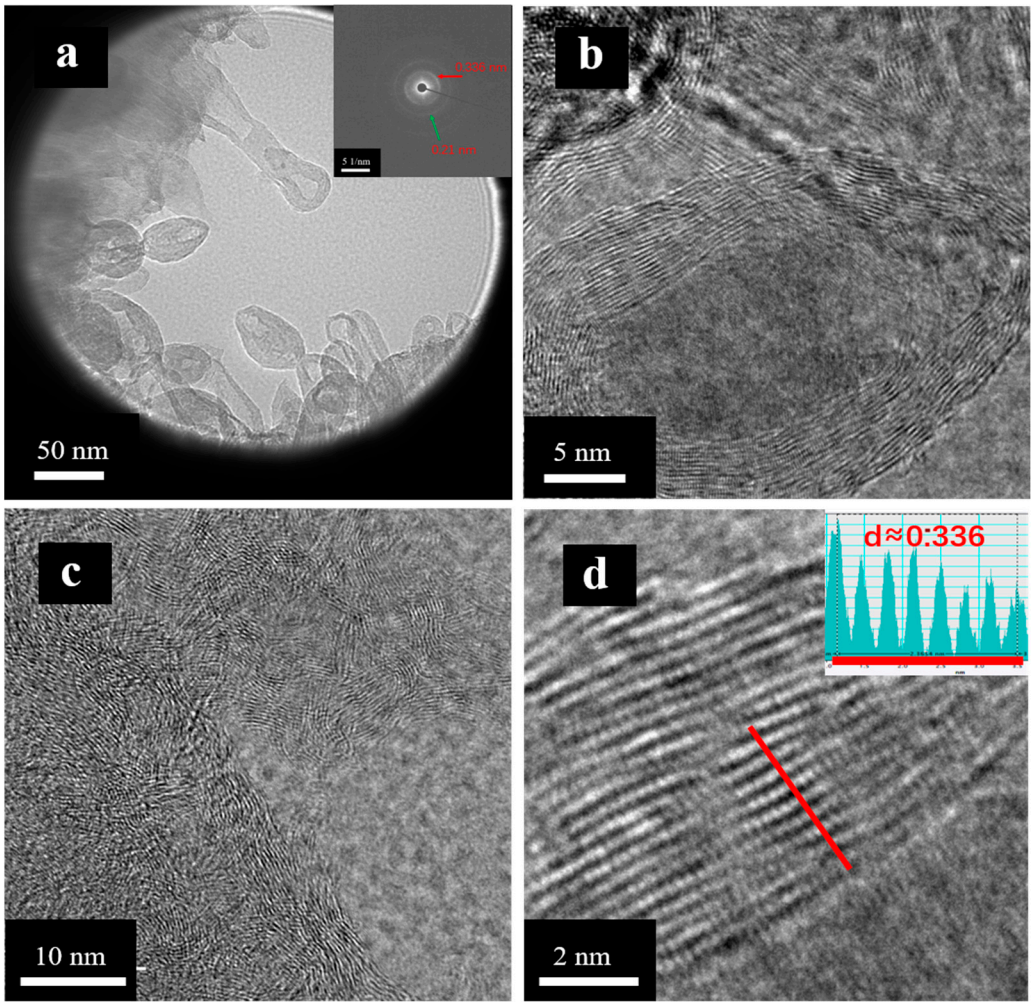

Figure 5. (**a**) TEM images of high-pressure synthesis of h-BN (tubular morphology structure) and SAED; (**b**) images of tubular structure; (**c**,**d**) TEM images of h-BN lattice structure.

As a comparison, the mixture of ammonium azide and nano boron powder was also compressed at 200 °C and 28 GPa, and, as was expected, the morphology of the samples differs greatly. The samples obtained at room temperature show a tubular morphology, while the samples obtained at a temperature of 200 °C show a sheet-like morphology. TEM results show that the obtained samples exhibit a h-BN sheet layer with a smooth surface (Figure 7a). In comparison to h-BN synthesized at ambient temperature, the h-BN obtained at 200 °C was well aligned. The SAED reveals multiple bright rings. EDS mapping confirms the uniform distribution of boron and nitrogen elements. The lattice distances of different diffraction rings were 0.336 nm, 0.21 nm, and 0.12 nm, corresponding to the (002), (110), and (100) crystal planes of h-BN, respectively. Figure 7b displays the well-aligned features of h-BN, indicating that thermal treatments can enhance crystallization. The

elevated temperature provides significant assistance in enhancing the reaction efficiency. This is primarily due to the accelerated mass transfer of materials and the promotion of continuous reactions between nanoboron and ammonium azide. As a result, the lamellar boron nitride is formed. In contrast, when the mixture of ammonium azide and nanoboron powder is compressed at room temperature, the reaction becomes localized. This localized reaction leads to the gradual formation of an isolation layer of h-BN due to compaction, which hinders further contact between ammonium azide and the internal boron particles. Consequently, this sequential process ultimately gives rise to the formation of h-BN with a tubular morphology on the surface of the boron particles.

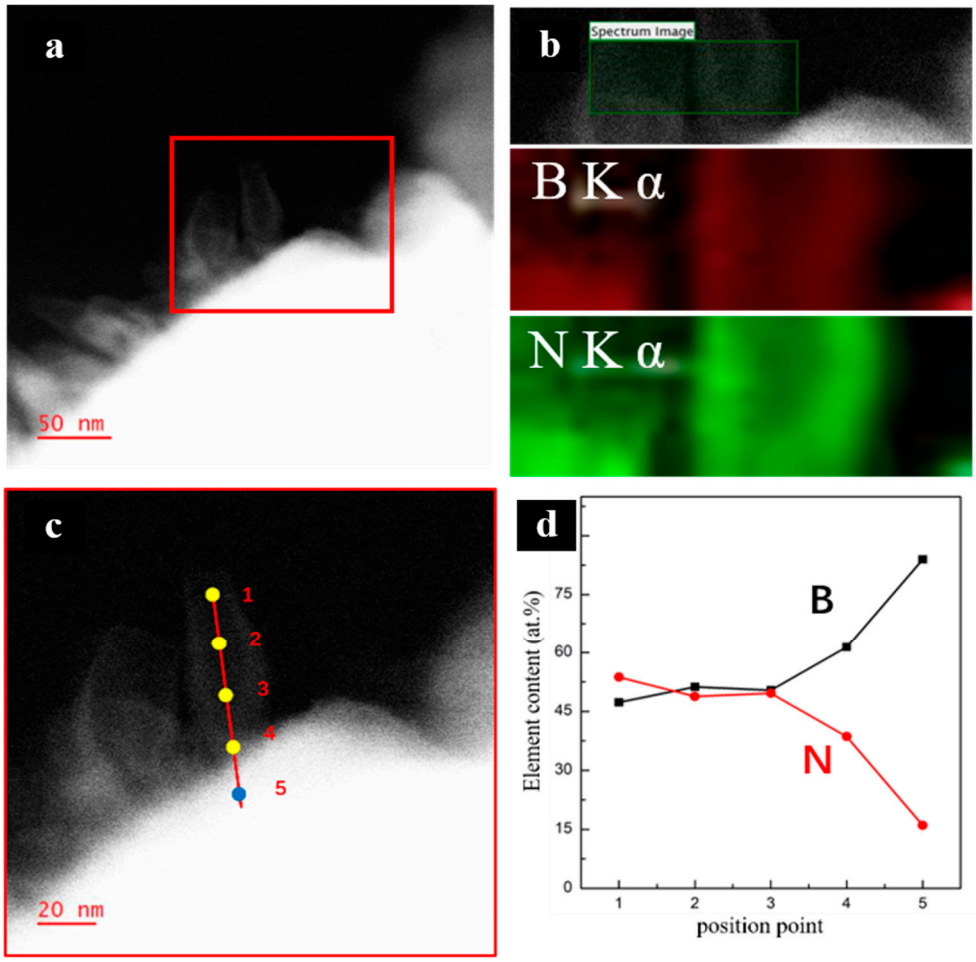

Figure 6. (**a**) STEM image of synthesized h-BN at room temperature and 28 GPa; (**b**) electron energy-loss spectrum (EELS) mapping of h-BN with tubular morphology (red box area); (**c**,**d**) proportional distribution of boron and nitrogen elements at different positions (yellow dots on tubular structure and blue dot on boron area).

The EELS spectra of the precursors and obtained samples were characterized to understand the bonding (Figure 7f). The precursor of nanoboron powder displays a prominent characteristic peak of boron (~188 eV) [45]. The absorption peak shows a diffuse scattering bump, implying an inferior crystallinity of nanoboron powder. No nitrogen characteristic peak protrusions are observed in the spectra, suggesting that the detected nitrogen–boron bonds are a result of the reaction between ammonium azide and boron powder. The EELS peaks' position of tubular h-BN obtained by room temperature and lamellar h-BN obtained with temperature assistance are consistent with those of commercial h-BN. The peaks of the samples match with the commercial h-BN containing typical B-N sp2 bonding, indicating the successful synthesis of sp2-bonded boron nitride under pressure.

The absorption peaks of the boron element can be sorted from low energy to high energy, with the π* bonds (189–195 eV) and σ* bonds (195–220 eV) exhibiting absorption. However, it is noteworthy that the π bond absorption peak of the h-BN with a tubular morphology is significantly higher than those of commercial h-BN and temperature-assisted samples. This phenomenon can be attributed to the relatively poor crystallinity of the h-BN with a tubular morphology synthesized at room temperature. The tubular morphology of h-BN requires a single layer with a certain curvature, leading to the presence of defects within the monolayer. These defects are characterized by disordered stacking between layers, as illustrated in Figure 5b [46,47].

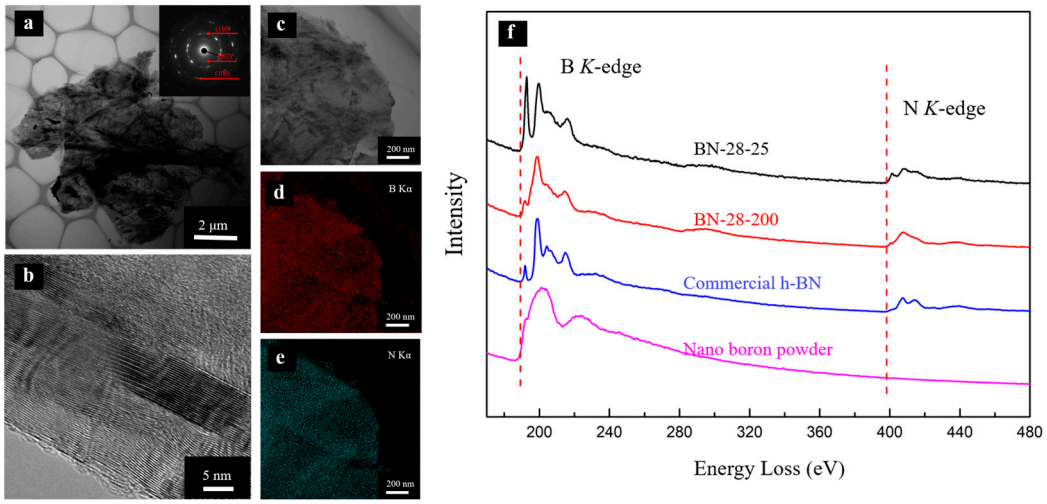

Figure 7. (**a**–**e**) STEM images of synthesized h-BN at 200 °C and 28 GPa; (**f**) electron energy-loss spectrum (EELS) of different samples.

4. Conclusions

In summary, we demonstrated a method for synthesizing h-BN with a tubular morphology at room temperature. In situ Raman measurements revealed a transition point of approximately 17.5 GPa for pressure-driven nitrogen–boron sp^2 bond formation. Additionally, a multianvil press was utilized to synthesize h-BN at a pressure of 28 GPa and ambient temperature. SEM and TEM studies confirmed that the morphology of the obtained h-BN was tubular, with dimensions ranging from 50 to 100 nanometers. Subsequently, high-pressure and thermal treatments were used to obtain crystalline h-BN, which also confirmed that the mechanism of room temperature compression to synthesize h-BN is different from that of obtaining samples using high pressure and temperature assistance. Under 28 GPa and 200 °C, high-crystallinity h-BN was obtained with a micro-size lamellar morphology. EELS was employed to precisely measure the composition and bonding states for those samples. The sample synthesized at ambient temperature and high pressure showed the typical sp^2-bonded boron and nitrogen peaks that exactly matched the EELS spectra of commercial h-BN. These results provide direct evidence that high pressure plays a crucial role in driving the nitrogen–boron reaction to form chemical bonds.

Supplementary Materials: The following supporting information can be downloaded at: https://www.mdpi.com/article/10.3390/cryst13081201/s1, Figure S1: XRD pattern of nanoboron powder. Figure S2. XRD pattern of ammonium azide. Figure S3. optical photos of samples and precursors. (a) nano boron powder; (b) sample obtained at 28 GPa and room temperature; (c) sample obtained at 28 GPa and 200 °C; (d) commercial h-BN. Figure S4. XRD pattern of the sample obtained at 28 GPa room temperature. Figure S5. (a,b) TEM images and size statistics (c,d) of tube-shaped h-BN for the sample obtained from 28 GPa and room temperature. Figure S6. (a) SEM images and size statistics (b) of boron paritles for the sample obtained from 28 GPa and room temperature. Figure S7. (a) Electron energy loss spectrum (EELS) mapping of nano boron powder and (b) commercial h-BN.

Figure S8. Quantitative analysis of EELS in different segments of commercial h-BN. Table S1.TEM-EDS results at different areas of sample obtained from 28 GPa and room temperature.

Author Contributions: H.G. and J.L. conceived and designed the experiments; D.J. performed the in situ high-pressure Raman experiment; J.L. and G.N. performed the multianvil press experiments; J.L. and P.M. conducted SEM and TEM testing and analyzed the data; J.L. wrote the paper. All authors have read and agreed to the published version of the manuscript.

Funding: This research was funded by the National Key Research and Development Program of China, grant numbers 2018YFA0703400/2018YFA0703404.

Data Availability Statement: Not applicable.

Conflicts of Interest: The authors declare no conflict of interest.

References

1. Naclerio, A.E.; Kidambi, P.R. A Review of Scalable Hexagonal Boron Nitride (h-BN) Synthesis for Present and Future Applications. *Adv. Mater.* **2023**, *35*, 2207374. [CrossRef]
2. Xu, H.; Ding, B.; Xu, Y.; Huang, Z.; Wei, D.; Chen, S.; Liu, B. Magnetically tunable and stable deep-ultraviolet birefringent optics using two-dimensional hexagonal boron nitride. *Nat. Nanotechnol.* **2022**, *17*, 1091–1096. [CrossRef]
3. Ramezani, F.; Parvez, S.; Fix, J.P.; Battaglin, A.; Whyte, S.; Borys, N.J.; Whitaker, B.M. Automatic detection of multilayer hexagonal boron nitride in optical images using deep learning-based computer vision. *Sci. Rep.* **2023**, *13*, 1595. [CrossRef]
4. Kim, M.; Pallecchi, E.; Ge, R.; Ge, R.; Wu, X.; Ducournau, G.; Lee, J.C.; Akinwande, D. Analogue switches made from boron nitride monolayers for application in 5G and terahertz communication systems. *Nat. Electron.* **2020**, *3*, 479–485. [CrossRef]
5. Moon, S.; Kim, J.; Park, J.; Im, S.; Kim, J.; Hwang, I.; Kim, J.K. Hexagonal Boron Nitride for Next-Generation Photonics and Electronics. *Adv. Mater.* **2023**, *35*, 2204161. [CrossRef] [PubMed]
6. Dean, C.R.; Young, A.F.; Meric, I.; Lee, C.; Wang, L.; Sorgenfrei, S.; Watanabe, K.; Taniguchi, T.; Kim, P.; Shepard, K.L. Boron nitride substrates for high-quality graphene electronics. *Nat. Nanotech.* **2010**, *5*, 722–726. [CrossRef]
7. Kim, D.P.; Moon, K.T.; Kho, J.G.; Economy, J.; Gervais, C.; Babonneau, F. Synthesis and characterization of poly (aminoborane) as a new boron nitride precursor. *Polym. Adv. Technol.* **1999**, *10*, 702–712. [CrossRef]
8. Xue, L.; Lu, B.; Wu, Z.S.; Ge, C.; Wang, P.; Zhang, R.; Zhang, X.D. Synthesis of mesoporous hexagonal boron nitride fibers with high surface area for efficient removal of organic pollutants. *Chem. Eng. J.* **2014**, *243*, 494–499. [CrossRef]
9. Hubáček, M.; Ueki, M.; Sato, T.; Brožek, V. High-temperature behaviour of hexagonal boron nitride. *Thermochim. Acta* **1996**, *282*, 359–367. [CrossRef]
10. Yang, H.; Wang, L.; Gao, F.; Dai, M.; Hu, Y.; Chen, H.; Zhang, J.; Qiu, Y.; Jia, D.; Zhou, Y.; et al. Shape evolution of two-dimensional hexagonal boron nitride single domains on Cu/Ni alloy and its applications in ultraviolet detection. *Nanotechnology* **2019**, *30*, 245706. [CrossRef] [PubMed]
11. Yang, H.; Wang, G.; Guo, Y.; Wang, L.; Tan, B.; Zhang, S.; Zhang, X.; Zhang, J.; Shuai, Y.; Lin, J.; et al. Growth of wafer-scale graphene–hexagonal boron nitride vertical heterostructures with clear interfaces for obtaining atomically thin electrical analogs. *Nanoscale* **2022**, *14*, 4204–4215. [CrossRef]
12. Tan, B.; Yang, H.; Hu, Y.; Gao, F.; Wang, L.; Dai, M.; Zhang, S.; Shang, H.; Chen, H.; Hu, P. Synthesis of high-quality multilayer hexagonal boron nitride films on Au foils for ultrahigh rejection ratio solar-blind photodetection. *ACS Appl. Mater. Interfaces* **2020**, *12*, 28351–28359. [CrossRef] [PubMed]
13. Wang, L.; Wu, B.; Jiang, L.; Chen, J.; Li, Y.; Guo, W.; Hu, P.; Liu, Y. Growth and etching of monolayer hexagonal boron nitride. *Adv. Mater.* **2015**, *27*, 4858–4864. [CrossRef] [PubMed]
14. Song, X.; Gao, J.; Nie, Y.; Gao, T.; Sun, J.; Ma, D.; Li, Q.; Chen, Y.; Jin, C.; Bachmatiuk, A.; et al. Chemical vapor deposition growth of large-scale hexagonal boron nitride with controllable orientation. *Nano Res.* **2015**, *8*, 3164–3176. [CrossRef]
15. Taniguchi, T.; Watanabe, K. Synthesis of high-purity boron nitride single crystals under high pressure by using Ba–BN solvent. *J. Cryst. Growth* **2007**, *303*, 525–529.
16. Zhigadlo, N.D. Crystal growth of hexagonal boron nitride (hBN) from Mg-B-N solvent system under high pressure. *J. Cryst. Growth* **2014**, *402*, 308–311. [CrossRef]
17. Gu, Y.; Zheng, M.; Liu, Y.; Xu, Z. Low-temperature synthesis and growth of hexagonal boron-nitride in a lithium bromide melt. *J. Am. Ceram. Soc.* **2007**, *90*, 1589–1591. [CrossRef]
18. Chen, L.; Gu, Y.; Li, Z.; Qian, Y.; Yang, Z.; Ma, J. Low-temperature synthesis and benzene-thermal growth of nanocrystalline boron nitride. *J. Cryst. Growth* **2005**, *273*, 646–650. [CrossRef]
19. Sun, J.; Lu, C.; Song, Y.; Ji, Q.; Song, X.; Li, Q.; Zhang, Y.; Zhang, L.; Kong, J.; Liu, Z. Recent progress in the tailored growth of two-dimensional hexagonal boron nitride via chemical vapour deposition. *Chem. Soc. Rev.* **2018**, *47*, 4242–4257. [CrossRef]
20. Heck, A.J.R.; Chandler, D.W. Imaging techniques for the study of chemical reaction dynamics. *Annu. Rev. Phy. Chem.* **1995**, *46*, 335–372.
21. Zhang, L.; Wang, Y.; Lv, J.; Ma, Y. Materials discovery at high pressures. *Nat. Rev. Mater.* **2017**, *2*, 17005. [CrossRef]

22. Utsumi, W.; Yagi, T. Light-transparent phase formed by room-temperature compression of graphite. *Science* **1991**, *252*, 1542–1544. [CrossRef]
23. Wang, Y.; Dong, X.; Tang, X.; Zheng, H.; Li, K.; Lin, X.; Fang, L.; Sun, G.; Chen, X.; Xie, L.; et al. Pressure-Induced Diels-Alder Reactions in C_6H_6-C_6F_6 Cocrystal towards Graphane Structure. *Angew. Chem. Int. Ed.* **2019**, *58*, 1468–1473.
24. Li, X.; Wang, T.; Duan, P.; Baldini, M.; Huang, H.T.; Chen, B.; Juhl, S.J.; Koeplinger, D.; Crespi, V.H.; Schmidt-Rohr, K.; et al. Carbon nitride nanothread crystals derived from pyridine. *J. Am. Chem. Soc.* **2018**, *140*, 4969–4972. [CrossRef] [PubMed]
25. Decker, D.L.; Bassett, W.A.; Merrill, L.; Hall, H.T.; Barnett, J.D. High-pressure calibration: A critical review. *J. Phys. Chem. Ref. Data* **1972**, *1*, 773–836. [CrossRef]
26. Shang, Y.C.; Shen, F.R.; Hou, X.Y.; Chen, L.-Y.; Hu, K.; Li, X.; Liu, R.; Tao, Q.; Zhu, P.-W.; Liu, Z.-D.; et al. Pressure Generation above 35 GPa in a Walker-Type Large-Volume Press. *Chin. Phys. Lett.* **2020**, *37*, 080701. [CrossRef]
27. Liu, Z.; Irifune, T.; Nishi, M.; Tange, Y.; Arimoto, T.; Shinmei, T. Phase relations in the system $MgSiO_3$–Al_2O_3 up to 52 GPa and 2000 K. *Phys. Earth Planet. Inter.* **2016**, *257*, 18–27. [CrossRef]
28. Liu, Z.; Nishi, M.; Ishii, T.; Fei, H.; Miyajima, N.; Ballaran, T.B.; Ohfuji, H.; Sakai, T.; Wang, L.; Shcheka, S.; et al. Phase relations in the system $MgSiO_3$-Al_2O_3 up to 2300 K at lower mantle pressures. *J. Geophys. Res-Sol. Ea.* **2017**, *122*, 7775–7788. [CrossRef]
29. Wu, X.; Cui, H.; Zhang, J.; Cong, R.; Zhu, H.; Cui, Q. High pressure synchrotron x-ray diffraction and Raman scattering studies of ammonium azide. *Appl. Phy. Lett.* **2013**, *102*, 121902. [CrossRef]
30. Kuzuba, T.; Era, K.; Ishii, T.; Sato, T. A low frequency Raman-active vibration of hexagonal boron nitride. *Solid State Commun.* **1978**, *25*, 863–865.
31. Saha, S.; Muthu, D.V.S.; Golberg, D.; Tang, C.; Zhi, C.; Bando, Y.; Sood, A.K. Comparative high pressure Raman study of boron nitride nanotubes and hexagonal boron nitride. *Chem. Phys. Lett.* **2006**, *421*, 86–90. [CrossRef]
32. Cuscó, R.; Pellicer-Porres, J.; Edgar, J.H.; Li, J.; Segura, A.; Artús, L. Pressure dependence of the interlayer and intralayer E_{2g} Raman-active modes of hexagonal BN up to the wurtzite phase transition. *Phys. Rev. B* **2020**, *102*, 075206.
33. Machon, D.; Bousige, C.; Alencar, R.; Torres-Dias, A.; Balima, F.; Nicolle, J.; de Sousa Pinheiro, G.; Souza Filho, A.G.; San-Miguel, A. Raman scattering studies of graphene under high pressure. *J. Raman Spectrosc.* **2018**, *49*, 121–129. [CrossRef]
34. Zhang, G.; Zhang, H.; Ninet, S.; Zhu, H.; Liu, C.; Itié, J.P.; Gao, C.; Datchi, F. Crystal structure and stability of ammonium azide under high pressure. *J. Phys. Chem. C* **2019**, *124*, 135–142. [CrossRef]
35. Zhang, G.; Zhang, H.; Ninet, S.; Zhu, H.; Beneut, K.; Liu, C.; Mezouar, M.; Gao, C.; Datchi, F. Transformation of Ammonium Azide at High Pressure and Temperature. *Materials* **2020**, *13*, 4102. [CrossRef] [PubMed]
36. Meng, Y.; Mao, H.K.; Eng, P.J.; Trainor, T.P.; Newville, M.; Hu, M.Y.; Kao, C.; Shu, J.; Hausermann, D.; Hemley, R.J. The formation of sp^3 bonding in compressed BN. *Nat. Mater.* **2004**, *3*, 111–114.
37. Ungar, T. Microstructural parameters from X-ray diffraction peak broadening. *Scr. Mater.* **2004**, *51*, 777–781. [CrossRef]
38. Harris KD, M.; Tremayne, M.; Kariuki, B.M. Contemporary advances in the use of powder X-ray diffraction for structure determination. *Angew. Chem. Int.* **2001**, *40*, 1626–1651. [CrossRef]
39. Jiang, H.X.; Lin, J.Y. Hexagonal boron nitride epilayers: Growth; optical properties and device applications. *ECS J. Solid State Sci. Technol.* **2016**, *6*, Q3012. [CrossRef]
40. Arenal, R.; Stephan, O.; Cochon, J.L.; Loiseau, A. Root-growth mechanism for single-walled boron nitride nanotubes in laser vaporization technique. *J. Am. Chem. Soc.* **2007**, *129*, 16183–16189. [CrossRef]
41. Lourie, O.R.; Jones, C.R.; Bartlett, B.M.; Gibbons, P.C.; Ruoff, R.S.; Buhro, W.E. CVD growth of boron nitride nanotubes. *Chem. Mater.* **2000**, *12*, 1808–1810. [CrossRef]
42. Ma, R.; Bando, Y.; Sato, T.; Kurashima, K. Growth, morphology, and structure of boron nitride nanotubes. *Chem. Mater.* **2001**, *13*, 2965–2971. [CrossRef]
43. Xiong, J.; Di, J.; Zhu, W.; Li, H. Hexagonal boron nitride adsorbent: Synthesis, performance tailoring and applications. *J. Energy Chem.* **2020**, *40*, 99–111.
44. Songfeng, E.; Wu, L.; Li, C.; Zhu, Z.; Long, X.; Geng, R.; Zhang, J.; Li, Z.; Lu, W.; Yao, Y. Growth of boron nitride nanotubes from magnesium diboride catalysts. *Nanoscale* **2018**, *10*, 13895–13901.
45. Otten, C.J.; Lourie, O.R.; Yu, M.F.; Cowley, J.M.; Dyer, M.J.; Ruoff, R.S.; Buhro, W.E. Crystalline boron nanowires. *J. Am. Chem. Soc.* **2002**, *124*, 4564–4565. [CrossRef]
46. Huang, J.Y.; Yasuda, H.; Mori, H. HRTEM and EELS studies on the amorphization of hexagonal boron nitride induced by ball milling. *J. Am. Ceram. Soc.* **2000**, *83*, 403–409. [CrossRef]
47. Berzina, B.; Trinkler, L.; Krutohvostov, R.; Williams, R.T.; Carroll, D.L.; Czerw, R.; Shishonok, E. Photoluminescence excitation spectroscopy in boron nitride nanotubes compared to microcrystalline h-BN and c-BN. *Phys. Status Solidi C* **2005**, *2*, 318–321.